Wavelet coefficients as a guide to DNA phase transitions

2009 EPL 87 38005

(http://iopscience.iop.org/0295-5075/87/3/38005)

A Letters Journal Exploring the Frontiers of Physics

August 2009

EPL, **87** (2009) 38005 www.epljournal.org
doi: 10.1209/0295-5075/87/38005

Wavelet coefficients as a guide to DNA phase transitions

R. F. Machado and G. Weber[a]

Department of Physics, Federal University of Ouro Preto - 35400 Ouro Preto-MG, Brazil

received 24 June 2009; accepted 20 July 2009
published online 24 August 2009

PACS 87.15.Zg – Biomolecules: structure and physical properties: Phase transitions
PACS 05.70.Fh – Thermodynamics: Phase transitions: general studies
PACS 87.14.gk – Biomolecules: types: DNA

Abstract – Physical statistics models such as the Peyrard-Bishop model are extensively used to study thermodynamic properties of DNA. One of the interesting aspects of this model is that it is a one-dimensional model exhibiting phase transitions which can be continuously changed from smooth to very sharp transitions. The partition function for the Peyrard-Bishop model can be calculated using the transfer integral technique yielding an eigenfunction which can be interpreted as a probability density. In this work we show that it is possible to expand the eigenfunction of the transfer integral operator using methods commonly used in wavelet signal analysis. The wavelet coefficients obtained from multiresolution analysis can be used as a tool to monitor the melting transition. This method is numerically very efficient and addresses the issue of eigenfunction localisation which can be employed in problems that make use of the transfer integral technique, demonstrating the application of wavelet multiresolution analysis in phase transition.

Introduction. – Modelling the DNA denaturation process both realistically and in a computationally efficient way remains to date a major challenge [1]. Calculated DNA melting temperatures are needed for a variety of technological applications, especially for techniques based on hybridisation to DNA probes in next-generation sequencing [2]. Probe design for instance requires the calculation of temperatures for a huge variety of DNA sequences [3], therefore coarse-grained models which allow for numerical efficiency are an attractive option. One of the most widely studied models, the Peyrard-Bishop model [4], was used successfully for the calculation of DNA melting temperatures [5] and a wealth of other applications [6–9].

In addition to its practical interest in describing the process of DNA denaturation, the Peyrard-Bishop model provides a framework for studying several aspects of thermodynamic phase transitions in one-dimensional systems. Notably, anharmonic formulations of the stacking interaction [10] as well as variants of the base-pair potentials [6,11] allow changing continuously from second- to first-order–type transitions [12]. Relevant thermodynamic variables can be calculated from this model by evaluating the classical partition function within the framework of the transfer integral method. For instance, the average base-pair stretching can be calculated as a function of temperature and is generally used as a criterion to determine the denaturation temperature.

This method results in an integral eigenequation whose eigenfunction can be interpreted as classical analogs of probability functions [13,14]. During the phase transition these eigenfunction change from strongly localised cusp-like functions to broadly distributed smooth functions. For first-order transitions this change is quite dramatical over a very short temperature range. In this work we use wavelet multiresolution analysis to follow the change of scale of the transfer integral eigenfunction. Multiresolution analysis is extensively used for processing edges in images. In this case a change of scale or resultion causes the loss of image details which can be monitored for edge detection. Here we show that a similar approach can be used to monitor the loss of detail caused by the change of scale of the eigenfunction during the phase transition. This method is numerically more efficient than the usual Gauss-Legendre quadrature method [13].

Theory. –

The model and the transfer integral method. The Peyrard-Bishop model [15] is defined by the Hamiltonian

$$H = \sum_i \frac{p_i^2}{2m} + W(y_i, y_{i-1}) + V(y_i), \qquad (1)$$

[a] E-mail: gweberbh@gmail.com

where $p_i = m\frac{\mathrm{d}y_i}{\mathrm{d}t}$ and m is the reduced mass of the i-th base pair. $V(y_i)$ describes the interaction between the base pairs and is given by the Morse potential

$$V(y_i) = D(e^{-ay_i} - 1)^2, \tag{2}$$

where D is the dissociation energy of the pair and a is a parameter whose inverse gives the range of the potential. The potential $W(y_i, y_{i-1})$ represents the stacking interaction between bases along the DNA molecule. To account for sharp melting transitions Dauxois *et al.* [10] proposed a anharmonic stacking interaction

$$W_a(y_i, y_{i-1}) = \frac{k}{2}\left[1 + \rho e^{-\alpha(y_i + y_{i+1})}\right](y_i - y_{i+1})^2, \tag{3}$$

where the exponential factor accounts for the fact that the molecular packing decreases with base opening. We will refer to this model as the anharmonic-Morse (AM) model.

In this work we also consider an alternative base-pair potential

$$V_s(y_i) = D(e^{-ay_i} - 1)^2 - f_s D\left[\tanh(y_i/\lambda_s)\right], \tag{4}$$

which models the formation of hydrogen bonds between the bases and the solvent whenever the distance between two paired bases exceeds a certain amount λ_s [11]. The factor f_s controls the barrier height of the combined potential. In this model the stacking interaction is given by an harmonic potential

$$W_h(y_i, y_{i-1}) = \frac{k}{2}(y_i^2 - 2y_i y_{i+1}\cos\theta + y_{i+1}^2), \tag{5}$$

where θ is the twist angle between neighboring bonds [11] which was introduced to avoid well known divergence problems in the partition function [13]. The Hamiltonian given by eqs. (4) and (5) also gives rise to a sharp denaturation [11], and we will refer to it as the harmonic-solvent (HS) model. Both models are representative of several variations of the original harmonic-Morse model [4] which have been proposed recently [6,16,17].

To obtain the equilibrium thermodynamical properties of the system we evaluate the configurational part of the canonical partition function

$$Z_y = \int \prod_{i=1}^{N+1} \mathrm{d}y_i \left[\prod_{i=1}^{N} \exp(-\beta K(y_i, y_{i+1}))\right], \tag{6}$$

and

$$K(y_i, y_{i+1}) = \frac{1}{2}W(y_i, y_{i+1}) + V(y_i). \tag{7}$$

The function Z_y can be calculated by means of the transfer integral (TI) method by defining a TI operator

$$\int_{-\infty}^{\infty} K(x, y)\varphi(y)\mathrm{d}y = \lambda\varphi(x), \tag{8}$$

where λ is an eigenvalue and $\varphi(x)$ its associated eigenvector. The average distance between two bases will be given by

$$\langle y\rangle = \frac{1}{Z_y}\sum_n \langle n|y|n\rangle \lambda_n^N, \tag{9}$$

where

$$\langle n|y|m\rangle \equiv \int \varphi_n(y) y \varphi_m(y)\mathrm{d}y. \tag{10}$$

The eigenfunction $|\varphi_n(y)|^2$ can be interpreted as a probability density and indeed the TI operator in eq. (8) can be mapped to a pseudo-Schrödinger equation [4]. For numerical purposes, we replace upper and lower limits of the improper integral in eq. (8) by y_{sup} and y_{inf} chosen such that outside this interval the probability density is negligibly small. This replacement, especially that of y_{sup}, is valid as long as there are localised (bound) states (eigenfunctions) whose identity and number depend on temperature. In fact, in the range from 80 K to 350 K there is only one localised state that becomes non-localised for high enough temperatures, signalling the melting of the molecule [13]. If the eigenvalues are sorted in descending order, this localised state is the first one and in the melting transition it is expected that $\lambda_1 \approx \lambda_2$. In the limit of very long molecules ($N \to \infty$) the partition function reduces to $Z_y = \lambda_1^N$ and $\langle y\rangle = \langle 1|y|1\rangle$ [4]. Also, we shift y by y_m, *i.e.* $y' = y + y_m$ such that the new lower limit becomes $y'_{\mathrm{inf}} = 0$. This is useful for the analysis which will be carried out in the next section since we will avoid negative values for y. To ease the notation, for the remaining sections of this letter y is always shifted by y_m, *i.e.* means y', unless noted otherwise.

The box spline expansion. By choosing a suitable method for numerical quadrature such as Gauss-Legendre, the integral in eq. (8) can be written as an eigenvalue problem (see, *e.g.*, [18]). Here, we propose an alternative approach to this problem using box spline expansion of the eigenfunction. The first step is to write the eigenfunctions in eq. (8) as

$$\varphi(x) = \sum_i c_i \phi_{i\ell}(x), \tag{11}$$

with

$$\phi_{i\ell}(x) = \frac{1}{\sqrt{\ell}}\phi\left(\frac{x - i\ell}{\ell}\right), \tag{12}$$

which is a contraction by the factor ℓ followed by a translation of $i\ell$ of a function $\phi(x)$ that has a compact suport (null outside an interval $[x_a, x_b]$). Functions of this kind are obtained by $p-1$ convolutions of the function $\mathbf{1}_{[0,1]}$ with itself are called box splines of degree p. One convolution ($p = 2$) yields

$$\phi(x) = \left\{\begin{array}{ll} x+1, & \text{if } -1 < x < 0 \\ 1-x, & \text{if } 0 < x < 1 \\ 0, & \text{otherwise} \end{array}\right\}, \tag{13}$$

with $x_a = -1$ and $x_b = 1$. In this case the support of $\phi_{i\ell}(x)$ is given by the closed interval $[(i-1)\ell, (i+1)\ell]$. Substitution of eq. (11) into eq. (8) gives

$$\sum_{i=1}^{M} c_i \int_{\Lambda_i} K(x,y)\phi_{i\ell}(x)\mathrm{d}y = \lambda \sum_{k=1}^{M} c_j \phi_{k\ell}(x), \tag{14}$$

where $\int_{\Lambda_i}$ denotes integration over the support of $\phi_{i\ell}(x)$ and M is the minimum number of translations necessary to cover the domain of $\varphi(x)$. Multiplying both sides of eq. (14) by $\phi_{j\ell}(x)$ and integrating over Λ_j we obtain the matrix equation

$$\mathbf{A}c = \lambda \mathbf{B}\mathbf{c}, \tag{15}$$

where the elements of the $M \times M$ matrix $\mathbf{A}$ are given by

$$A_{ij} = \int_{\Lambda_j}\int_{\Lambda_i} \phi_{j\ell}(x)K(x,y)\phi_{i\ell}(y)\mathrm{d}y\mathrm{d}x, \tag{16}$$

and the elements of $\mathbf{B}$ by

$$B_{ij} = \int_{\Lambda_i \cap \Lambda_j} \phi_{i\ell}(x)\phi_{j\ell}(x)\mathrm{d}x, \tag{17}$$

and $\mathbf{c}$ is the $M \times 1$ matrix whose elements are the coefficients c_i in eq. (11). The elements B_{ij} will be null whenever $\Lambda_i \cap \Lambda_j = \emptyset$. This property renders the matrix $\mathbf{B}$ symmetric band-diagonal. For $\phi(x)$ given by eq. (13) we have

$$\mathbf{B} = \frac{1}{6}\begin{pmatrix} 4 & 1 & 0 & \cdots & 0 \\ 1 & 4 & 1 & \cdots & 0 \\ \vdots & \ddots & \ddots & \ddots & \vdots \\ 0 & \cdots & 1 & 4 & 1 \\ 0 & \cdots & 0 & 1 & 4 \end{pmatrix}. \tag{18}$$

So, the original problem turns into the generalised eigenvalue problem in eq. (15). The matrices $\mathbf{A}$ and $\mathbf{B}$ are both symmetric and sparse. This is obvious for matrix $\mathbf{B}$ for $M \gg 1$. Numerical evaluation of eq. (16) shows that the largest elements of $\mathbf{A}$ are of order 10^{-2} while the smallest ones are of order 10^{-18}. If we assume that elements smaller than the cutoff 10^{-13} are null we end up having to calculate only between 14 and 18 percent of the $M \times M$ elements. These properties turns this problem into a natural candidate to be handled by the Lanczos method [19]. In this iterative method only extreme eigenpairs are calculated with good precision and that is just what we need since we are interested only in the largest eigenvalues. The only operation involving the matrices in the Lanczos algorithm are multiplications by vectors, which can be accomplished in a very efficient way because we can take advantage of the structure of $\mathbf{B}$ and of techniques for dealing with sparse matrices such as *row-indexed sparse storage mode* [20].

The average base-pair stretching $\langle y \rangle$, eq. (9), can now be evaluated as a function of ℓ

$$\langle y_\ell \rangle = \frac{\ell}{6}\sum_i c_i \left[(i-1)c_{i-1} + 4ic_i + (i+1)c_{i+1}\right]. \tag{19}$$

Another useful quantity to characterise the phase transition which is closely related to the average stretching is the average fraction of closed bonds. We say that the i-th base pair is open if y_i is greater than a reference value y_{ref}. From eq. (9) one can see that this fraction is given by

$$f = \int_{y_{\mathrm{inf}}}^{y_{\mathrm{ref}}} \varphi(y)^2 \mathrm{d}y, \tag{20}$$

which yields

$$f = \mathbf{c}_m^T \mathbf{B}_m \mathbf{c}_m, \tag{21}$$

where $\mathbf{c}_m$ is the vector obtained from $\mathbf{c}$ by taking only its first m elements, $\mathbf{c}_m^T$ is its transpose and $\mathbf{B}_m$ is the matrix that one obtains when the matrix $\mathbf{B}$ is restricted to its first m lines and columns. Since $f = 1$ for $m = M$ from eq. (17), f close to 1 implies the vanishing of the elements c_i of $\mathbf{c}$ for $i \geqslant m$.

Wavelet coefficients. The approach outlined in the previous section allows us to obtain an additional tool to characterise the phase transition of thermal denaturation which is based on the multiresolution analysis used in signal processing [21]. In this technique a certain signal $f(x)$ can be viewed at different scales by means of the expansion

$$f(x) = \sum_i a_\ell[i]\phi_{i\ell}(x), \tag{22}$$

where

$$a_\ell[i] = \langle f(x)\phi_{i\ell}(x)\rangle = \int_{-\infty}^{+\infty} f(x)\phi_{i\ell}(x)\mathrm{d}x \tag{23}$$

and $\phi_{i\ell}(x)$ is given by eq. (12). In the jargon of wavelet analysis ϕ is called the scaling function. When one changes the resolution from ℓ to 2ℓ the new coefficients will be given by

$$a_{2\ell}[i] = \sum_{n=-\infty}^{\infty} a_\ell[n]h[n-2i], \tag{24}$$

with

$$h[n] = \frac{1}{\sqrt{\pi}}\int_{-\pi}^{+\pi} \frac{\hat{\phi}(2\omega)}{\hat{\phi}(\omega)}\exp(in\omega), \tag{25}$$

where $\hat{\phi}(\omega)$ is the Fourier transform of $\phi(x)$. The reverse is also true, that is, given the Fourier transform of $h[n]$

$$\hat{h}(\omega) = \sum_{n=-\infty}^{+\infty} h[n]\exp(-in\omega), \tag{26}$$

$\hat{\phi}(\omega)$ will be given by

$$\hat{\phi}(\omega) = \prod_{p=1}^{+\infty} \frac{h(2^{-p}\omega)}{\sqrt{2}}. \tag{27}$$

One can show that [21]

$$\hat{h}(\omega) = \sqrt{2}\exp\left(\frac{-i\epsilon\omega}{2}\right)\left(\cos\frac{\omega}{2}\right)^p, \tag{28}$$

with p positive integer and $\epsilon = 0$ for p even and $\epsilon = 1$ for p odd, renders

$$\hat{\phi}(\omega) = \exp\left(\frac{-i\epsilon\omega}{2}\right)\left(\frac{\sin(\omega/2)}{\omega/2}\right)^p, \tag{29}$$

which is the Fourier transform of a box spline of degree $p-1$. The signal in eq. (22) has another decomposition given by

$$f(x) = \sum_i \tilde{a}_\ell[i]\tilde{\phi}_{i\ell}(x), \tag{30}$$

in a space $\tilde{\mathbf{V}}_\ell$ orthogonal to $\mathbf{V}_\ell$ whose basis is given by $\{\tilde{\phi}_{i\ell}(x)\}_{i\in Z}$. The Fourier transform of the scaling function $\tilde{\phi}(x)$ can be obtained by the same method as $\hat{\phi}(\omega)$ but with

$$\hat{\tilde{h}}(\omega) = \sqrt{2}\exp\left(\frac{-i\epsilon\omega}{2}\right)\left(\cos\frac{\omega}{2}\right)^{\tilde{p}} \times \sum_{k=0}^{q-1}\binom{q-1+k}{k}\left(\sin\frac{\omega}{2}\right)^{2k}, \tag{31}$$

instead of $\hat{h}(\omega)$ in eq. (27), where $q = (p+\tilde{p})/2$ and $\tilde{p}$ is a free parameter. This parameter gives the number of vanishing moments of the wavelet function

$$\psi(x) = \sqrt{2}\sum_{n=-\infty}^{+\infty}(-1)^{1-n}\tilde{h}[1-n]\phi(2x-n). \tag{32}$$

This function plays an essential role in the multiresolution analysis, since the set $\{\psi_{i2\ell}(x)\}_{i\in Z}$ with

$$\psi_{i2\ell}(x) = \frac{1}{\sqrt{2l}}\psi\left(\frac{x}{2\ell} - i\right), \tag{33}$$

is a basis for the space $\mathbf{W}_{2\ell}$ orthogonal to $\mathbf{V}_{2\ell}$ such that $\mathbf{V}_\ell = \mathbf{V}_{2\ell} \oplus \mathbf{W}_{2\ell}$. The details lost due to the change from the resolution ℓ to the coarser 2ℓ are given by the coefficients

$$d_{2\ell}[i] = \langle\psi_{i2\ell}(x)f(x)\rangle = \sum_{n=-\infty}^{\infty} a_\ell[n]g[n-2i], \tag{34}$$

with $g[n] = (-1)^{1-n}\tilde{h}[1-n]$. We will show in the next section that these coefficients can be used as tools to characterize the phase transition that takes place during the DNA thermal denaturation.

Results and discussion. – For the AM model we used the following parameters $D = 0.04\,\text{eV}$, $a = 4.5\,\text{Å}^{-1}$, $y_m = 0.3\,\text{Å}$, $k = 0.06\,\text{eV/Å}^2$ and $\alpha = 0.35\,\text{Å}^{-1}$ and $M = 2^9 = 512$. For the HS model we used the additional parameters $f_s = 0.1$ and $\theta = 0.01\,\text{rad}$. We used as integration limits $y'_{\text{inf}} = 0.0$ and $y'_{\text{sup}} = 30\,\text{Å}$, corresponding to a resolution $\ell = (y'_{\text{sup}} - y'_{\text{inf}})/M = 0.058\,\text{Å}$. For the matrices in eq. (21) we used $m = M/10$ which corresponds to y_{ref} of 3.0 Å.

Depending on the parameters used, both the anharmonic-Morse (AM) model and the harmonic-solvent (HS) model display either sharp first-order or smooth second-order transitions. For instance, for the AM model the order of the transition is characterized by the anharmonicity parameter ρ in eq. (3). For large values of ρ the model exhibits sharp transitions while for low values a much smoother transition is obtained [12]. The phase transition is usually characterized by an increase of the average stretching $\langle y\rangle$ or by the decrease of the average fraction of open hydrogen bonds f. In fig. 1 we show our calculations of the average stretching and average fraction of open bonds for the AM model using the box spline expansion of eq. (11). These results are numerically very close to other implementations using Gauss-Legendre integration quadratures [13] which confirms the reliabilty of this method.

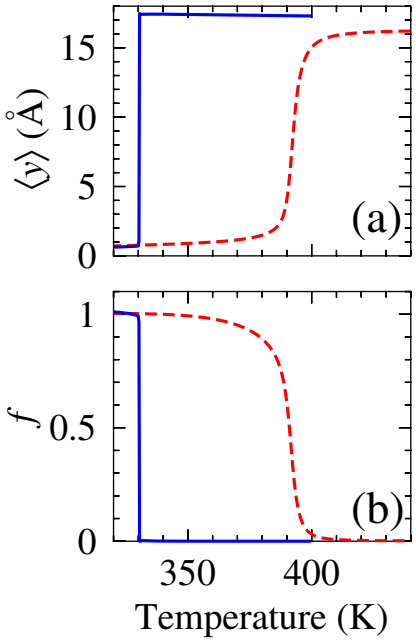

Fig. 1: (Colour on-line) (a) Average stretching as a function of temperature and (b) fraction of open bonds for the AM model for two different values of the anharmonic parameter $\rho = 0.5$ (dashed red line) and $\rho = 1.5$ (blue line).

The phase transition can also be characterized by the spatial localization of the eigenfunction $\varphi(x)$ [13,22]. This eigenfunction is strongly localized around the equilibrium position y_m for low temperatures and broadly distributed along the potential plateau for high temperatures. This behaviour is illustrated in fig. 2 where we show $\varphi(x)$ for the AM model using a second-order–type anharmonic parameter. At low temperatures the eigenfunction is completely confined to the potential well and gradually distributes over a broader region as the temperature increases. However, if we choose a larger anharmonic parameter, this change of eigenfunction localization takes place over a very narrow range of temperatures as show in fig. 3.

For both orders of phase transition, the eigenfunctions at low temperatures exhibit a cusp like singularity

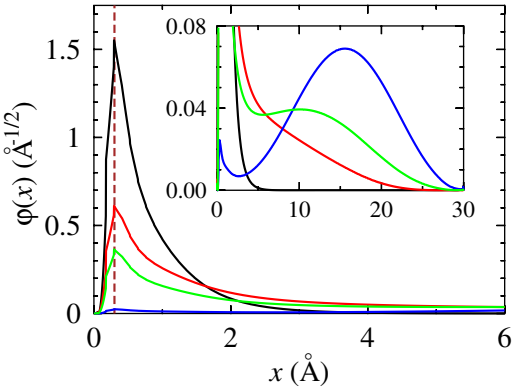

Fig. 2: (Colour on-line) Eigenfunctions $\varphi(x)$ for the second-order–type parameter $\rho = 0.5$ at four different temperatures: 340 K (black line), 390 K (red line), 392 K (green line), and 400 K (blue line). The vertical dashed line shows the distance y_m and the inset shows long-range details of the eigenfunction.

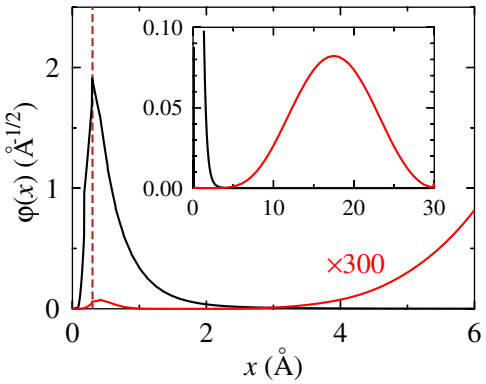

Fig. 3: (Colour on-line) Eigenfunctions $\varphi(x)$ for the first-order–type parameter $\rho = 1.5$ at two different temperatures: 330 K (black line) and 330.5 K (red line, scaled by a factor of 300). The vertical dashed line shows the distance y_m and the inset shows long-range details of the eigenfunction.

centered at y_m. The presence of this singularity is ideally suited to be quantified by means of the wavelet coefficients $d_{2\ell}$ in eq. (34). If the wavelets in eq. (34) have $\tilde{p}$ moments, that is, if

$$\int_{-\infty}^{+\infty} x^k \psi(x) \mathrm{d}x = 0, \quad \text{for} \quad 0 \leqslant k < \tilde{p} \tag{35}$$

then $d_{2\ell}$ will be very small, provided ℓ is very small as well and $f(x)$ is locally $\mathbf{C}^k$ (k-times differentiable) with $k < \tilde{p}$. This is indeed the case since if $f(x)$ is locally $\mathbf{C}^k$, then it can be approximated by a polynomial of degree k over a small interval. Choosing $\tilde{p} = p = 2$, and $f(x) = \varphi(x)$ in eq. (34), the resulting coefficients allow us to monitor the evolution of the cusp singularity of the eigenfunction $\varphi(x)$. Essentially, all we need to do is to perform the summation in eq. (34) with $a_\ell[n]$ replaced by c_n that are the components of the eigenvector $\mathbf{c}$ in eq. (15). The coefficients $\tilde{h}[n]$ depend only on p and $\tilde{p}$ [21]. For our

Table 1: Coefficients $g[n]$ for the AM model.

n	$g[n]$
−3, 5	0.03314563036812
−2, 4	0.06629126073624
−1, 3	−0.17677669529664
0, 2	−0.41984465132951
1	0.99436891104358

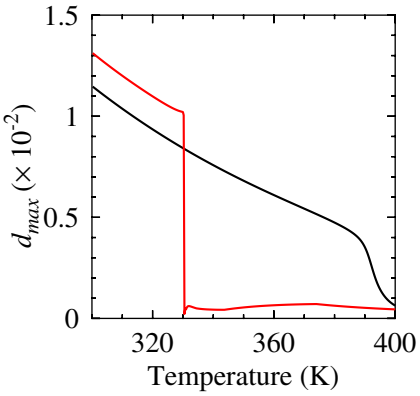

Fig. 4: (Colour on-line) Largest wavelet coefficient for first-order (red line) and second-order (black line) parameters as function of temperature.

choice parameters there are only nine non-null coefficients shown in table 1. In fig. 4 we show the largest wavelet coefficient as function of temperature for the two types of phase transition of the AM model. One can see that the vanishing of the cusp singularity at the transition for the first-order phase transition is reflected by an abrupt fall of $d_{\max}$ with temperature. On the other hand, the smooth behaviour of $d_{\max}$ with temperature for second-order phase transitions signals the persistence of the cusp singularity and the eventual flattening of the eigenfunction $\varphi(x)$ in the transition region. For high temperatures in both cases we obtain low values of $d_{\max}$ reflecting the appropriateness of approximating a smooth curve (the bell-like curve in fig. 2 and fig. 3) by a polynomial with degree less than 4 over small intervals.

The harmonic-solvent (HS) model has sharp first-order transitions for large values of λ_s in eq. (4), see figs. 5a and b and results in ref. [11]. In contrast to the AM model where the first-order transition is caused by the anharmonicity of the stacking potential, for the HS model this transition is caused by the solvent base-pair potential. In other words, the first-order transitions of these models have completely different origins. Therefore, if the wavelet coarsening loss coefficient $d_{\max}$ truly monitors the eigenfunction cusp this should also be true for the HS model. This is indeed the case as shown in fig. 5c. This supports the conclusion that the anharmonicity in the AM model and the solvent term HS model give rise the same kind of transition namely a transition characterised by the

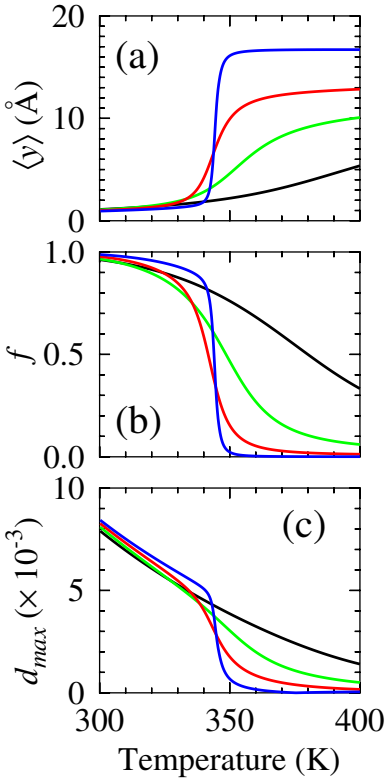

Fig. 5: (Colour on-line) (a) Average stretching, (b) fraction of closed bonds and (c) largest wavelet coefficient as a function of temperature for the HS model. Four different values of the parameter λ_s were used (in Å): 1.0 (black line); 3.0 (green line); 5.0 (red line) and 10.0 (blue line).

flattening of the eigenfunction $\varphi(x)$ and the persistence, or absence, of its the cusp singularity at equilibrium position of the Morse potential.

Conclusion. – The wavelet coefficient allows us to distinguish the transitions that fall in either category in a quantitative way. These transitions are qualitatively different from the one that takes place for high values of ρ in the AM model. In this case the transition is really sharp with the cusp singularity of the eigenfunction $\varphi(x)$ vanishing in a very narrow range of temperatures. The absence of flattening of $\varphi(x)$ in this case signals the strong cooperativity of the transition. These physical scenarios are quite different and determining which is the one that fits the thermal denaturation is essential for our understanding of this process.

* * *

One of us (GW) would like to thank Fapemig and CNPq for financial support.

REFERENCES

[1] Peyrard M., *Nat. Phys.*, **2** (2006) 13.
[2] Shendure J. and Ji H., *Nat. Biotechnol.*, **26** (2008) 1135.
[3] Haslam N., Whiteford N., Weber G., Prügel-Bennett A., Essex J. W. and Neylon C., *PLoS ONE*, **3** (2008) e2500.
[4] Peyrard M. and Bishop A. R., *Phys. Rev. Lett.*, **62** (1989) 2755.
[5] Weber G., Haslam N., Whiteford N., Prügel-Bennett A., Essex J. W. and Neylon C., *Nat. Phys.*, **2** (2006) 55.
[6] Peyrard M., Cuesta-López S. and Angelov D., *J. Phys.: Condens. Matter*, **21** (2009) 034103.
[7] Alexandrov B., Voulgarakis N. K., Rasmussen K. Ø., Usheva A. and Bishop A. R., *J. Phys.: Condens. Matter*, **21** (2009) 034107.
[8] Joyeux M. and Florescu A.-M., *J. Phys.: Condens. Matter*, **21** (2009) 034101.
[9] De Luca J., Drigo Filho E., Ponno A. and Ruggiero J. R., *Phys. Rev. E*, **70** (2004) 026213.
[10] Dauxois T., Peyrard M. and Bishop A. R., *Phys. Rev. E*, **47** (1993) R44.
[11] Weber G., *Europhys. Lett.*, **73** (2006) 806.
[12] Theodorakopoulos N., Dauxois T. and Peyrard M., *Phys. Rev. Lett.*, **85** (2000) 6.
[13] Zhang Y.-L., Zheng W.-M., Liu J.-X. and Chen Y. Z., *Phys. Rev. E*, **56** (1997) 7100.
[14] Cuesta J. A. and Sánches A., *J. Stat. Phys.*, **115** (2004) 869.
[15] Peyrard M., *Nonlinearity*, **17** (2004) R1.
[16] Joyeux M. and Buyukdagli S., *Phys. Rev. E*, **72** (2005) 051902.
[17] Saccomandi G. and Sgura I., *J. R. Soc. Interface*, **3** (2006) 655.
[18] Weber G., Haslam N., Essex J. W. and Neylon C., *J. Phys.: Condens. Matter*, **21** (2009) 034106.
[19] Parlett B. N., *The Symmetric Eigenvalue Problem* (Siam) 1998.
[20] Press W. H. *et al.*, *Numerical Recipes in C*, 2nd edition (Cambridge University Press, Inc.) 1992.
[21] Mallat S., *A Wavelet Tour of Signal Processing*, 2nd edition (Academic Press) 1999.
[22] Dauxois T. and Peyrard M., *Phys. Rev. E*, **51** (1995) 4027.